JOURNAL OF SOLID STATE CHEMISTRY 90, 31–41 (1991)

A New Barium Titanium (III) Pyrophosphate: $BaTi_2(P_2O_7)_2$

SHUMIN WANG AND SHIOU-JYH HWU*

Department of Chemistry, Rice University, P.O. Box 1892, Houston, Texas 77251

Received April 12, 1990; in revised form August 3, 1990

The new barium titanium (III) pyrophosphate $BaTi_2(P_2O_7)_2$ has been prepared by conventional high temperature solid state reaction at 900°C in a fused silica tube. $BaTi_2(P_2O_7)_2$ crystallizes with four formula units in a cell with dimensions $a = 10.680(3)$ Å, $b = 10.564(4)$ Å, $c = 9.834(4)$ Å, $\beta = 102.88(3)°$ and $V = 1081.6(6)$ Å^3 in space group $C_{2h}^6 - C_{2/c}$ (No. 15) of the monoclinic system. The single crystal structure refinement gives a final structure solution with R index on F_o^2 of 0.018 for 99 variables and GOF = 1.05. $BaTi_2(P_2O_7)_2$ displays a new layered type structure which consists of layers of slightly distorted TiO_6 octahedra with (P_2O_7) and (BaO_{10}) polyhedra between the layers. The structural framework is built up from corner-sharing TiO_6 octahedra and P_2O_7 pyrophosphate groups, to give rise to $[Ti_2(P_2O_7)_2]^{2-}$ units and to form tunnels where the barium cations reside. Magnetic susceptibility measurements on selected single crystals confirm the presence of Ti^{3+} (d^1) ions with spin $S = \frac{1}{2}$. The high oxidative thermal stability of $BaTi_2(P_2O_7)_2$ versus the stabilities of other trivalent titanium cation-containing compounds, including Ti_2O_3, $TiPO_4$, and $BaTi_2(PO_4)_3$, owing to possible anion matrix effects are discussed.

Introduction

Over the years much attention has been devoted to the phosphates, silicates, and silicophosphates of almost all the metallic elements in the periodic table. These microporous solids are involved in various applications such as catalysts, molecular sieves, or ion exchangers, to name a few. Some of the ion exchangers with open framework tunnel structures exhibit fast ion conduction. In examples from the NASICON (Na Superionic Conductor) family, the silicon-doped series of composition $Na_{1+x}Zr_2Si_xP_{3-x}O_{12}$ (*1*, *2*) offers conductivity that is competitive with the best β- and β''-alumina solid electrolytes (*3–5*).

Syntheses of reduced early transition metal phosphate compounds have resulted in a large collection of structurally interesting inorganic compounds with open framework structures. By using a lithium insertion reaction of $KTi_3P_6Si_2O_{25}$ which has a two-dimensional tunnel structure, a reduced compound containing titanium (3+) cations was reportedly prepared, e.g., $KLi_2Ti_3P_6Si_2O_{25}$ (*6*). Two forms of reduced sodium titanium (III) pyrophosphates, namely α- and β-$NaTiP_2O_7$, were isolated from conventional solid state high temperature reactions (*7*). NASICON-related frameworks involving the mixed valence Ti^{III}–Ti^{IV} are known in the compounds of $Na_xTi_2(PO_4)_3$ ($x = 1 \sim 3$) (*8*), $K_{2-x}Ti_2(PO_4)_3$ ($0 \leq x \leq 0.5$), $M_2Ti_2(PO_4)_3$ (M = Rb and Tl) (*9*), and $MTi_2(PO_4)_3$ (M = Ca, Sr, Ba) (*10*). The

* To whom correspondence should be addressed.

0022-4596/91 $3.00

structures of these reduced compounds are characteristically composed of a mixed framework built up from corner-sharing titanium octahedra (TiO_6) and phosphate (PO_4) or pyrophosphate (P_2O_7) units. Recently a new phosphate, $Mg_3Ti_4P_7O_{24}$, containing a mixed (Ti, Mg) O_6 octahedron was reported (*11*).

In searching for new low valent early transition metal phosphates and to exploit the thermal stabilities of oxyanions of the PO_4^{3-} and $P_2O_7^{4-}$ types, the system BaO–TiO_x–P_2O_5 ($x \leq 1.5$) was investigated. In this paper we describe the synthesis, X-ray single crystal structure, magnetic properties, and thermal analysis of the new Ti (III) phosphate compound, namely barium titanium pyrophosphate, $BaTi_2(P_2O_7)_2$.

Experimental

Syntheses. The syntheses of single crystals were carried out using barium titanate, titanium metal (powder form), and phosphorus pentaoxide as starting materials. Polycrystalline samples of Ba_2TiO_4 (*12*) were prepared by a solid state reaction of Aldrich barium carbonate (99.98%) and titanium oxide (99.9+ %) and calcined at 1100°C in air. Reaction of Ba_2TiO_4, Ti (Aldrich, 99.9%), and P_2O_5 (Mallinckrodt, 99. + %) in a molar ratio of 1 : 2 : 4 in an evacuated silica tube at 900°C for 72 hr followed by slow cooling at a rate of −5°C/hr to room temperature resulted in a large number of gem-like navy blue crystals.

Attempts to prepare high purity polycrystalline $BaTi_2(P_2O_7)_2$ were carried out in two steps at temperatures ranging from 800 to 1000°C. The temperature at which the data crystal was grown, 900°C, was also found to be the best condition for preparing stoichiometric samples. The first step of the synthesis is to prepare a solid state precursor with a nominal composition of $BaTi_{1.5}(P_2O_7)_2$. This was calcined in air from reaction mixtures of $BaCO_3$, TiO_2, and $(NH_4)_2HPO_4$ (Fisher Scientific Co., 99.4%) at 900 ~ 1000°C. A reduction reaction was then carried out from a stoichiometric reaction of $BaTi_{1.5}(P_2O_7)_2$ and Ti in fused silica for 3 days. The reaction products were higher than 95% in purity on the basis of the X-ray powder diffraction (XRD) analysis. It is noted that some impurities due to black phases (<5% yield) were found in polycrystalline samples. The powder XRD patterns of selected black phases, however, showed a close relationship with that of the title compound. Semiquantitative analysis of these black crystals with the microprobe of an EDAX-equipped Hitachi S570 scanning electron microscope showed the presence of Ba, Ti, and P. Single crystal structure attempts of the black phases as yet are unsuccessful.

Single crystal X-ray structure determination. A blue gem-like crystal, with average dimensions 0.10 × 0.25 × 0.40 mm, was selected for indexing and intensity data collection on a Rigaku AFC5S four circle diffractometer (Mo$K\alpha$ radiation, λ = 0.71069 Å) equipped with a graphite monochrometer. Crystallographic data collection parameters are tabulated in Table I. The unit cell parameters and the orientation matrix for data collection were determined by least squares fit of 25 peak maxima with $7° < 2\theta < 20°$. There was no detectable decay according to three reflections (−2, −2, 0; 1, −3, −1; −2, 0, 2) that were measured every 100 reflections during data collection. The TEXSAN (*13*) software package was used for crystal structure solution and refinement. Data reduction, intensity analysis, and space group determination were accomplished with the program PROCESS and resulted in a Laue class of 2/*m*. On the basis of the intensity statistics, systematic extinctions (*hkl*: $h + k = 2n$; o*o*l: $l = 2n$), and the successful solution and structure refinement, the space group was determined to be $C_{2/c}$ (No. 15). Empirical absorption corrections based on three (2θ = 17.11°, 25.14°, and 27.02°) azimuthal scans were ap-

TABLE I

CRYSTAL DATA FOR $BaTi_2P_4O_{14}$

Formula mass (amu)	581.02
Space group	C_{2h}^6, $C_{2/c}$ (No. 15)
a (Å)	10.680 (3)
b (Å)	10.564 (4)
c (Å)	9.834 (4)
β (degree)[a]	102.88 (3)
V (Å^3)	1081.6 (6)
Z	4
T (K) of data collection	296
ρ_{calc} (g cm^{-3})	3.57
Radiation (graphite monochromated)	Mo$K\alpha$ (λ = 0.71069 Å)
Crystal shape, color	Gem-like, navy blue
Crystal size (mm)	0.10 × 0.25 × 0.40
Linear absorption coefficient (cm^{-1})	56.97
Transmission factors	0.69–1.00
Scan type	$\omega - 2\theta$
Scan speed (deg min^{-1})	4.0
Scan range (deg.)	−0.7 to 0.7 in ω
Background counts	¼ of scan range on each side of reflection
2θ (max)	55°
Data collected	$+h, +k, \pm l$
p for σ (F^2)	0.05
No. of unique data ($F_0^2 > 0$)	1141
No. of unique data with $F_0^2 > 3\sigma(F_0^2)$	1122
F_{000}	1088
$R(F^2)$	0.018
$R_w(F^2)$	0.032
R (on F for $F_0^2 > 3\sigma(F_0^2)$)	0.050
No. of variables	99
Error in observed unit weight (e^2)	1.05

[a] α and γ were constrained to be 90° in the refinement of cell constants.

plied to the intensity data. The atomic coordinates were found using the program SHELX-86 (*14*). The structure and thermal parameters were then refined by full-matrix least-squares methods based on F^2 to R = 0.018, R_w = 0.032, and GOF = 1.05. The occupancy factor for barium atoms was initially refined but the resultant value indicated full occupancy. The final positional and thermal parameters are given in Table II[1] and the selected bond distances are listed in Table III.

[1] See NAPS document No. 04799 for 9 pages of supplementary materials. Order from ASIS/NAPS, Microfiche Publications, P.O. Box 3513, Grand Central Station, New York, NY 10163. Remit in advance $4.00 for microfiche copy or for photocopy $7.75 up to 20 pages plus $.30 for each additional page. All orders must be prepaid.

Powder X-ray diffraction. Powder X-ray diffraction patterns of the polycrystalline samples were recorded at room temperature on a Philips PW 1840 diffractometer with Cu$K\alpha$ radiation and an Ni filter. NBS (National Bureau of Standards) silicon was mixed with the sample and used for an internal standard. The XRD powder patterns ($5° \leq 2\theta \leq 60°$) were indexed and refined by the least squares program LATT (*15*) with constraint to the monoclinic crystal system. The refined lattice parameters of fifty-six reflections are a = 10.683(4) Å, b = 10.574(3) Å, c = 9.835(3) Å, and β = 102.90(4)°, which are in excellent agreement with those of the single crystal structure (Table I).

Magnetic susceptibility. Susceptibility measurements were carried out in a VTS-50 susceptometer (SHE Corp., San Diego, CA); this instrument is located at Northwestern University and operates in the temperature range 0 ~ 400 K and 0–5 T. The selected blue crystals were contained in a quartz basket which was suspended by a cotton thread from the VTS sample translator drive. The temperature and field dependence of the susceptibility of the basket were previously determined and their effect was negligible in the present experiments. The susceptometer was calibrated with National Bureau of Standards Al and Pt standard samples.

The magnetic susceptibility, χ, of selected single crystals is plotted versus temperature from 4.95 to 345.5 K in Fig. 1. These data were least-squares fitted to the Curie–Weiss relation,

$$\chi = \chi_0 + C/(T - \theta),$$

including a term contributed from the temperature-independent paramagnetism and diamagnetism, χ_0; a Curie–Weiss contribution from the Ti^{3+} (d^1) magnetic moments; Curie constant, C; and Weiss constant, θ. The least squares fit of the curve gives χ_0 = 0.0130(10) emu/gm, C = 1.36(3) emu K/gm,

TABLE II

POSITIONAL AND EQUIVALENT THERMAL PARAMETERS FOR $BaTi_2P_4O_{14}$

Atomic Parameters

Atom	Wyckoff notation	x	y	z	B_{eq} (Å^2)[a]
Ba	4d	$\frac{1}{4}$	$\frac{1}{4}$	$\frac{1}{2}$	1.25(1)
Ti(1)	4e	0	0.55098(7)	$\frac{1}{4}$	0.48(2)
Ti(2)	4a	0	0	0	0.41(3)
P(1)	8f	0.05937(7)	0.31190(7)	0.05899(7)	0.48(2)
P(2)	8f	0.27932(7)	0.45628(7)	0.20234(7)	0.49(2)
O(1)	8f	0.0680(2)	0.3365(2)	−0.0893(3)	0.99(6)
O(2)	8f	−0.0348(2)	0.4017(2)	0.1073(2)	0.83(7)
O(3)	8f	0.0214(2)	0.1770(2)	0.0821(2)	0.89(7)
O(4)	8f	0.1979(2)	0.3287(2)	0.1596(2)	0.76(7)
O(5)	8f	0.3519(2)	0.4867(2)	0.0917(2)	1.09(8)
O(6)	8f	0.1820(2)	0.5598(2)	0.2084(2)	0.87(7)
O(7)	8f	0.3641(2)	0.4194(2)	0.3413(2)	0.89(7)

Thermal Parameters[b]

Atom	U_{11}	U_{22}	U_{33}	U_{12}	U_{13}	U_{23}
Ba	0.0073(2)	0.0112(2)	0.0287(2)	0.00070(8)	0.0032(1)	0.0066(1)
Ti(1)	0.0066(3)	0.0058(3)	0.0060(3)	0	0.0015(3)	0
Ti(2)	0.0046(3)	0.0045(3)	0.0065(3)	−0.0002(2)	0.0015(2)	0.0002(3)
P(1)	0.0060(3)	0.0045(3)	0.0072(3)	−0.0006(2)	0.0003(3)	−0.0002(2)
P(2)	0.0054(3)	0.0067(4)	0.0067(3)	−0.0010(3)	0.0013(3)	−0.0002(3)
O(1)	0.018(1)	0.012(1)	0.009(1)	0.0034(9)	0.0035(8)	0.0020(8)
O(2)	0.010(1)	0.009(1)	0.012(1)	0.0000(8)	0.0017(8)	−0.0036(8)
O(3)	0.013(1)	0.007(1)	0.014(1)	−0.0031(8)	0.0025(8)	−0.0007(8)
O(4)	0.0054(9)	0.007(1)	0.015(1)	−0.0002(8)	−0.0018(7)	0.0001(8)
O(5)	0.013(1)	0.016(1)	0.014(1)	−0.0037(9)	0.0075(8)	−0.0007(9)
O(6)	0.009(1)	0.009(1)	0.015(1)	−0.0007(8)	0.0026(8)	−0.0011(8)
O(7)	0.012(1)	0.012(1)	0.008(1)	−0.0032(8)	−0.0019(8)	0.0000(8)

[a] Anisotropically refined atoms are given in the form of the isotropic equivalent displacement parameter defined as $B_{eq} = \frac{4}{3}[a^2\beta_{11} + b^2\beta_{22} + c^2\beta_{33} + (2ac\cos\beta)\beta_{13}]$.

[b] The general temperature-factor expression of an atom for a given set of planes (hkl) is $\exp[-2\pi^2(U_{11}h^2a^{*2} + U_{22}k^2b^{*2} + U_{33}l^2c^{*2} + 2U_{13}hla^*c^*\cos\beta^*]$; where the U_{ij} are the thermal parameters expressed in terms of mean-square amplitudes of vibration in angstroms.

and $\theta = -2.96(1)$ K. The calculation of Bohr magnetons (B.M.) was done using the formula

$$\mu_{eff} = 2.84 \times \sqrt{C}\ (\text{B.M.}),$$

and resulted in $\mu_{eff} = 3.31$ for two single spin d^1 (Ti^{3+}) or 1.66 per Ti^{3+}. (The spin-only value is 1.73 B.M. for a single free electron.) This suggests that an unpaired electron in each titanium cation is electronically localized. However, if one sights along the χ vs T curve, one can feature a possible Néel transition occurring at $T_N \sim 260$ K. It might be due to the weak magnetic spin coupling between d^1 sites induced from the shortest Ti–Ti distance, e.g., $\frac{1}{2}c = 4.92$ Å.

TABLE III

IMPORTANT BOND DISTANCES (Å) AND ANGLES (°) FOR $BaTi_2P_4O_{14}$

	TiO_6 Octahedra		
Ti(1)—O(1)	1.981(2) (2×)	Ti(2)—O(3)	2.029(2) (2×)
Ti(1)—O(2)	2.089(2) (2×)	Ti(2)—O(5)	1.993(2) (2×)
Ti(1)—O(6)	2.087(2) (2×)	Ti(2)—O(7)	2.063(2) (2×)
O(1)—Ti(1)—O(1)	106.2(1)	O(3)—Ti(2)—O(3)	180.00
O(2)—Ti(1)—O(2)	81.9(1)	O(5)—Ti(2)—O(5)	180.00
O(6)—Ti(1)—O(6)	174.9(1)	O(7)—Ti(2)—O(7)	180.00
O(1)—Ti(1)—O(2)	86.49(9) (2×)	O(3)—Ti(2)—O(5)	85.16(9) (2×)
O(1)—Ti(1)—O(2)	165.38(9) (2×)	O(3)—Ti(2)—O(7)	85.35(9) (2×)
O(1)—Ti(1)—O(6)	86.37(9) (2×)	O(5)—Ti(2)—O(7)	82.87(9) (2×)
O(1)—Ti(1)—O(6)	90.57(9) (2×)		
O(2)—Ti(1)—O(6)	86.35(8) (2×)		
O(2)—Ti(1)—O(6)	97.52(9) (2×)		
	PO_4 Tetrahedra in P_2O_7 units		
P(1)—O(1)	1.505(2)	P(2)—O(4)	1.609(2)
P(1)—O(2)	1.533(2)	P(2)—O(5)	1.504(2)
P(1)—O(3)	1.513(2)	P(2)—O(6)	1.511(2)
P(1)—O(4)	1.596(2)	P(2)—O(7)	1.512(2)
O(4)—P(1)—O(1)	109.4(1)	O(4)—P(2)—O(5)	109.0(1)
O(4)—P(1)—O(2)	108.7(1)	O(4)—P(2)—O(6)	106.5(1)
O(4)—P(1)—O(3)	104.7(1)	O(4)—P(2)—O(7)	101.5(1)
O(1)—P(1)—O(2)	112.3(1)	O(5)—P(2)—O(6)	109.8(1)
O(1)—P(1)—O(3)	112.6(1)	O(5)—P(2)—O(7)	114.0(1)
O(2)—P(1)—O(3)	108.7(1)	O(6)—P(2)—O(7)	115.2(1)
P(1)—O(4)—P(2)	128.9(1)		
	BaO_{10} Polyhedron		
Ba—O(2)	2.807(2) (2×)		
Ba—O(3)	2.934(2) (2×)		
Ba—O(5)	3.049(3) (2×)		
Ba—O(6)	3.067(2) (2×)		
Ba—O(7)	2.823(2) (2×)		

Further examination for this possible magnetic ordering in relationship to the structure transformation is underway.

Thermogravimetric analysis (TGA). Thermal analyses (by DuPont 9900 Thermal Analysis System) were carried out in an oxygen atmosphere with the flow rate of 30 ml/min and heating rate of 10°C/min. A platinum pan was used for containing the powder samples. The analysis (20 ~ 950°C) of ca. 20 mg polycrystalline sample showed that $BaTi_2(P_2O_7)_2$ was decomposed (according to the following equation) to the two known

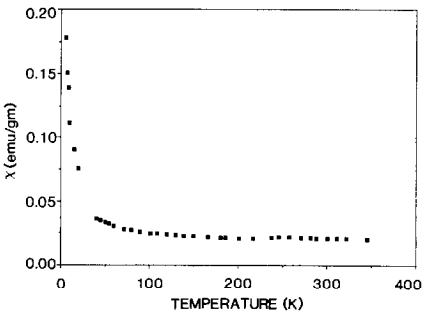

FIG. 1. Magnetic susceptibility (χ) of $BaTi_2(P_2O_7)_2$ uncorrected for the diamagnetism of the constituent atoms, plotted as a function of temperature.

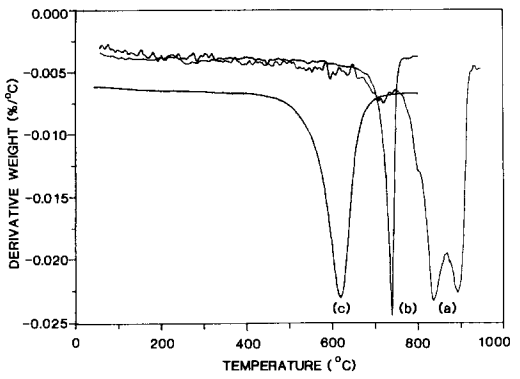

FIG. 2. Thermogravimetric analysis curves of Ti(III)-containing compounds. The first derivative curves, $\Delta wt/\Delta T$ (%/°C), of (a) $BaTi_2(P_2O_7)_2$, (1×), (b) $TiPO_4$, (0.21×), and (c) Ti_2O_3, (0.17×) are plotted as the function of temperature (K) to show their oxidative decomposition behavior (see text).

titanium (4+)-containing phosphates which were identified by XRD patterns (*16*):

$$2BaTi_2(P_2O_7)_2 + O_2 \rightarrow 2BaTiP_2O_8 + 2TiP_2O_7.$$

The net weight gain due to the oxidative decomposition is in a good agreement with that of the theoretical value, 2.62% vs 2.75%, respectively, within experimental error.

One of the major interests of the compound $BaTi_2(P_2O_7)_2$ rests on its relatively high oxidative thermal stability examined by the thermogravimetric analysis method. As shown in Figure 2, the $\Delta wt/\Delta T$ (%/°C) curves (Fig. 2, curves a, b, and c) of the compounds $BaTi_2(P_2O_7)_2$, $TiPO_4$, and Ti_2O_3, respectively, are plotted as a function of temperature. The decomposition temperatures are obtained from the peak minimum of the curves a, b, c. In curve a, for $BaTi_2(P_2O_7)_2$, two peaks at the temperatures of 835 and 890°C are shown in approximately equal intensities to implicate a two-step decomposition process which is attributed to two crystallographically dissimilar trivalent titanium cations. The differences in Ti–O bond strength and bond interactions between TiO_6 octahedra and pyrophosphate P_2O_7 (see the next section) may justify the formations of the oxidative decomposition products $BaTiP_2O_7$ and TiP_2O_7 and in turn give rise to two different decomposition temperatures. Nonetheless, the high decomposition temperatures result in high oxidative thermal stability in $BaTi_2(P_2O_7)_2$ as is evident compared with the decomposition temperatures of $TiPO_4$ (735°C, Fig. 2 curve b) and Ti_2O_3 (620°C, Fig. 2 curve c). The trend in increasing order of the thermal stability of Ti_2O_3, $TiPO_4$, and $BaTi_2(P_2O_7)_2$ may be due to the combination of the anion matrix effect, (P_2O_7) for example, and the incorporation of the electropositive cations (Ba^{2+}). Furthermore, the measured decomposition temperature of a similar reduced ternary phosphate, $BaTi_2(PO_4)_3$, ca. 800°C, is also consistently high.

It is noted that a small peak in curve a of Fig. 2 is shown at ca. 730°C, which suggests that the pseudobinary phase $TiPO_4$ is present in the polycrystalline sample. The impurity level is less than 3% according to the ratio of the integrated intensities.

Results and Discussion

As shown in Fig. 3, the extended crystal structure of the title compound is viewed along the *b*-axis. The resulting host framework consists of nearly rectangular tunnels running along the [010] direction with barium atoms sitting along the two-fold axis. A monoclinic unit cell is outlined with solid lines. The unit cell dimensions are a = 10.680(3) Å, b = 10.564(4) Å, c = 9.834(4) Å, and β = 102.88(3)° (Table I). Despite the complicated structure, the formula $BaTi_2(P_2O_7)_2$ itself can be self-explanatory, i.e., barium and titanium cations are isolated in the anion matrix that is built up from the double pyrophosphates, $(P_2O_7)_2$. The single crystal structure determination reveals that the structural framework consists of corner-

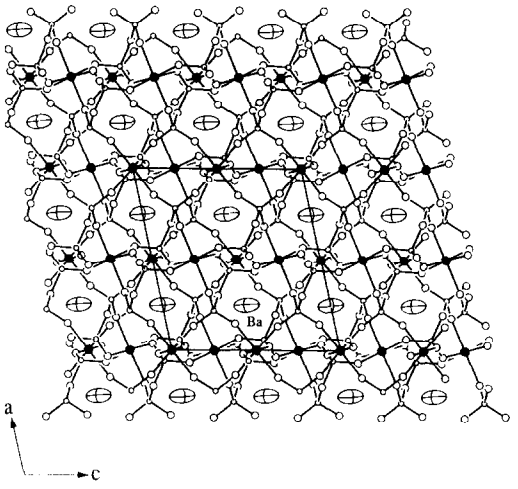

FIG. 3. The projected ORTEP drawing of the extended structure of $BaTi_2(P_2O_7)_2$ is viewed along b. The barium atoms are drawn at 90% probability. The solid circles represent titanium atoms whereas the large and small open circles are oxygen and phosphorus atoms, respectively. The projected unit cell on the ac-plane is outlined.

sharing titanium octahedra (TiO_6) and pyrophosphate (P_2O_7) groups, which gives rise to tunnels where the barium cations reside. Furthermore, the shape of the tunnel reflects the elongation of the Ba thermal ellipsoids ($U_{33} > U_{22} > U_{11}$).

The unit cell structure is shown in Fig. 4, with Ti–O bonds drawn in thick lines and P–O bonds in thin lines. The barium atoms are omitted for clarity. It is immediately apparent that in this structure the TiO_6 octahedra form parallel layers along the bc-plane and two neighboring layers are interconnected by (P_2O_7) units to form a $(Ti_2P_4O_{14})^{2-}$ slab. Two types of titanium metal cations (Ti1 and Ti2) in TiO_6 octahedra are alternatively arranged along the (200) planes in a manner similar to that in the α-L-TiP_2O_7 (*17*) structure. A schematic representation of the layered arrangement of α-L-TiP_2O_7 is shown in Fig. 5. Groups of covalently bonded pyrophosphate anions, $P_2O_7^{4-}$, are sharing corner oxygen atoms with TiO_6 octahedra to bind the layers together. It is noted that the interlayer separation, d_L, of the two adjacent titanium planes is greatly governed by the bond arrangement between TiO_6 and P_2O_7 groups and the configuration of the pyrophosphate anion. In the idealized structure of α-L-TiP_2O_7 (Fig. 5), P–O–P bonds are shown to be linear and perpendicular to the planes. This arrangement is the result of corner-sharing of all three terminal oxygen atoms, O_t, in one PO_4 tetrahedron with that of TiO_6 octahedra in one plane. To the contrary, the O_t's in $[Ti_2(P_2O_7)_2]^{2-}$ slabs of the $BaTi_2(P_2O_7)_2$ structure are bonded to the titanium atoms in different planes (Fig. 4). Consequently, the P–O–P bond angle is bent (see later discussion) to result in a much smaller layer separation, $d_L = d_{200} = 5.21$ Å, compared to 6.94 Å for TiP_2O_7 (*17*).

The crystallographic difference between the two titanium sites comes from the fact that the $Ti(1)O_6$ octahedron is linked to four

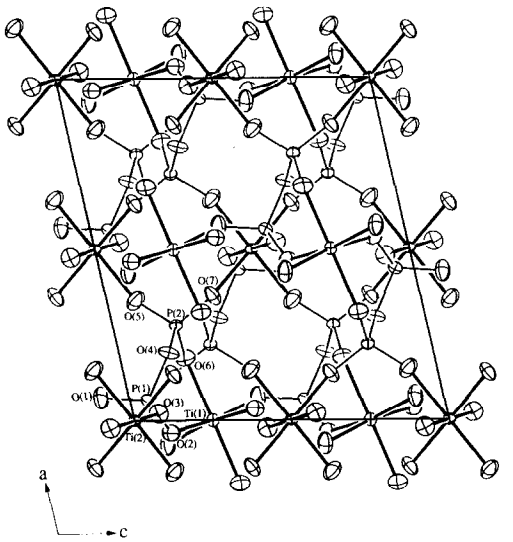

FIG. 4. The ORTEP drawing of the projected unit cell of $BaTi_2(P_2O_7)_2$ along b. Barium atoms are omitted for clarity. The TiO_6 octahedra are drawn in heavy lines and all the atoms are drawn at 90% probability. The atom labelings are corresponding to the positional parameters listed in Table II.

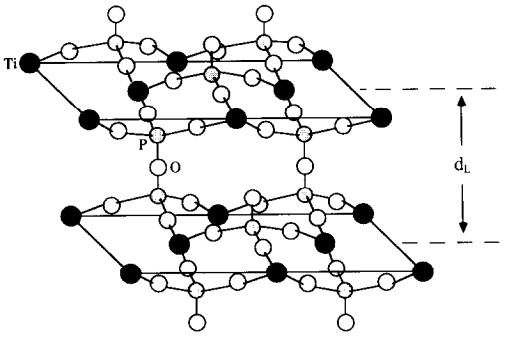

FIG. 5. Schematic representation of an idealized structure of α-L-TiP_2O_7. Titanium metal cations are alternatively arranged along the planes. The interlayer separation, d_L, is 6.94 Å for TiP_2O_7 compared to 5.21 Å for $BaTi_2(P_2O_7)_2$ (see text).

(P_2O_7) versus six in $Ti(2)O_6$ to form $[Ti(P_2O_7)_4]$ and $[Ti(P_2O_7)_6]$ units, respectively. Each pyrophosphate (P_2O_7) shares two oxygen atoms, O(2) and O(6), with the same $Ti(1)O_6$ octahedron to form a Ti(1)–O(2)–P_2O_5–O(6)–Ti(1) linkage, as shown in Fig. 6. A second (P_2O_7) unit shares the oxygen atoms in the same manner and is related to the first (P_2O_7) unit by a twofold symmetry. The units are then linked together in three dimensions by the remaining phosphate oxygens, e.g., O(1) to

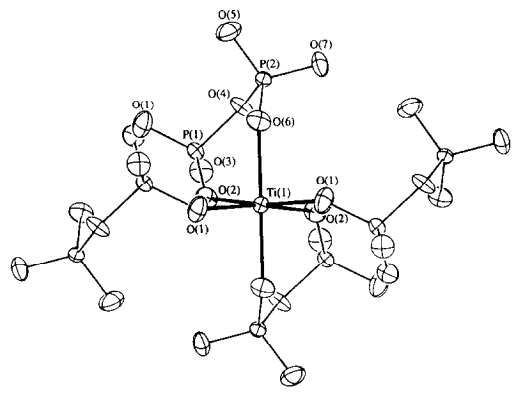

FIG. 6. The ORTEP drawing of $[Ti(P_2O_7)_4]$ unit in the structure of $BaTi_2(P_2O_7)_2$.

the symmetry-related Ti(1) and O(3), O(5), O(7), to Ti(2), to form the $[Ti_2(P_2O_7)_2]^{2-}$ framework (Figs. 3 and 6).

The TiO_6 octahedra are slightly distorted with bond distances and selected O–Ti–O bond angles listed in Table III. Starting with $Ti(1)O_6$ the point symmetry at the central Ti metal cation is C_2. The octahedron consists of two short and four long titanium–oxygen bonds with distances of ca. 1.98 and 2.09 Å, respectively. A strong correlation between electrostatic interaction and bond distance is evident. The short Ti–O bonds correspond to the doubly coordinated oxygen atoms, O(1), which are coordinated to titanium and phosphorous cations only. The long bonds correspond to the triply coordinated oxygen atoms, O(2) and O(6), due to the coordination of an additional barium cation.

The second titanium cation Ti(2) forms a $Ti(2)O_6$ octahedron, which has a point symmetry of C_i at the center. Thus, all the oxygen atoms and associated Ti–O bonds are related by an inversion center. Note that the Ti–O bond length in $Ti(2)O_6$ ranges from 1.99 to 2.06 Å, and is somewhat more homogeneous than that in the $Ti(1)O_6$ octahedron, e.g., 1.98 ~ 2.09 Å. This may be attributed to the fact that each and every one of the oxygen atoms in the $Ti(2)O_6$ octahedron have equal coordination numbers (C.N. = 3). Nevertheless, the observed titanium–oxygen bond distances in the present structure are consistent with the sum of Shannon crystal radii (2.07 Å) of six-coordinate Ti^{3+} (0.810 Å) and O^{2-} (1.26 Å) (*18*), as well as the reported Ti–O bond distances in various reduced titanium phosphates (*7–11*), ranging from 1.91 to 2.14 Å.

The structure of the bridging pyrophosphate unit, P_2O_7, is constructed by two PO_4 tetrahedra bridged by the corner oxygen atom, O(4), and has a nearly eclipsed configuration (Fig. 7). The least square plane view of the P_2O_7 configuration shows a P(1)–O(4)–P(2) angle of 128.9(1)° (Fig. 7a).

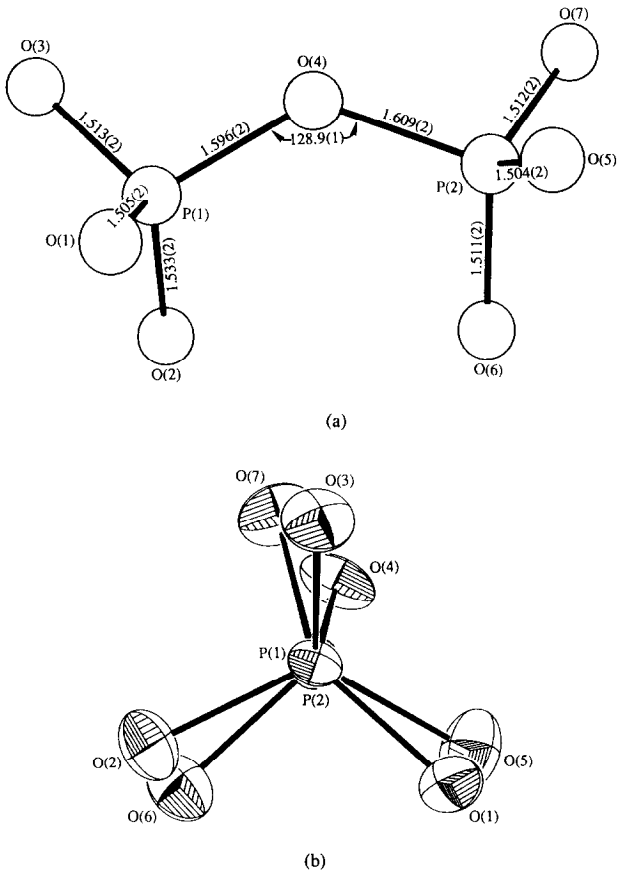

FIG. 7. A pyrophosphate group in $BaTi_2(P_2O_7)_2$. (a) A least square plane view and (b) view parallel to the P(1)–P(2) vector.

The six nonbridging oxygen atoms are essentially naked and available for Ti–O bonding in the previously discussed TiO_6 octahedra. The P–O bond distances (1.505–1.609 Å) and O–P–O angles (101.5–115.2°), as listed in Table III, are quite diverse, which indicates that the phosphorus atoms are displaced from the center of their tetrahedron. The averaged bond distance of the bridging P–O bond is calculated to be 0.09 Å longer than that of terminal P–O. This is very likely due to electrostatic interaction as well as a steric effect induced by a rather small P–O–P angle.

This difference in bond length distribution, in a distorted polyhedron, can be qualitatively correlated to and in turn justified by the electrostatic interaction that each individual oxide anion in the (P_2O_7) unit undergoes. That is, the coordinated cations (Ba^{2+}, Ti^{3+}, and P^{5+}) determine the bond strengths of the oxide anions. The bond strengths, ρ_x [= (No. of positive charges)/C.N.], that each cation contributes are 0.20 for Ba^{2+}, 0.50 for Ti^{3+}, and 1.25 for P^{5+}. Then, the predicted P–O distances for the (P_2O_7) unit can be calculated by the equation given by Baur (*19*):

$$d(\text{P–O})(\text{in Å}) = 1.537 + 0.109\ \Delta\rho_0,$$

TABLE IV

OBSERVED AND CALCULATED P—O DISTANCES IN $BaTi_2(P_2O_7)^2$

Anion	ρ_0	$\Delta\rho_0$	d_{obs} (Å)	d_{calc} (Å)	$\lvert\Delta d\rvert$
P(1)—O(1)	1.75	−0.29	1.505	1.505	0.000
P(1)—O(2)	1.95	−0.09	1.533	1.527	0.006
P(1)—O(3)	1.95	−0.09	1.513	1.527	0.014
P(1)—O(4)	2.50	+0.46	1.596	1.587	0.009
Mean	2.04				
P(2)—O(4)	2.50	+0.41	1.609	1.582	0.027
P(2)—O(5)	1.95	−0.14	1.505	1.522	0.017
P(2)—O(6)	1.95	−0.14	1.511	1.522	0.011
P(2)—O(7)	1.95	−0.14	1.512	1.522	0.010
Mean	2.09				

where $\Delta\rho_0$ is the difference between the ρ_x of one individual oxide and the mean ρ_0 of all oxides in the coordination polyhedron. The mean P–O distance, 1.537 Å, is an empirically derived constant by Baur. The predicted P–O distances are compared with the observed values in Table IV. The deviation in $|\Delta d|$ is attributed in part to the difference in charge separation of Ba–O and Ti–O, which is not considered in Baur's equation. Nevertheless, the results are generally satisfactory.

The barium cations are coordinated with 10 oxygen atoms at distances ranging from 2.81 to approximately 3.07 Å (Fig. 8). The configuration of the BaO_{10} polyhedron has a C_i-symmetry. It is important to note that this electropositive divalent cation cooperatively leads the formation of a double $[Ti_2(P_2O_7)_2]^{2-}$ framework as opposed to the monovalent sodium cation in the formation of a single $[TiP_2O_7]^{1-}$ framework in β-NaTi P_2O_7 (7). Consequently, the titanium cations are reduced in both compounds from the tetravalent to the trivalent oxidation state.

In conclusion, the structure of $BaTi_2(P_2O_7)_2$ can be described as an extended two-layer slab, $[Ti_2P_4O_{14}]^{2-}$, with the barium cations residing in the tunnels that are constructed by TiO_6 octahedra and pyrophosphate P_2O_7. In the structure unit of $[Ti(P_2O_7)_4]$, the unusual feature of two "bidentate" pyrophosphate P_2O_7 ligands, each of which shares two oxygen atoms (one from each PO_4 tetrahedra), is shown for the first time. The use of rigid and bulky oxyanions has resulted in the compounds characterized by structurally isolated and electronically localized Ti^{3+} (d^1) cations. Such compounds offer a great opportunity for an examination of their physical properties in regard to the magnetic behavior of the titanium cation, because the interaction between titanium metal cations is simplified. The oxidative thermal stability of the two trivalent titanium atoms in the reduced barium titanopyrophosphate, $BaTi_2(P_2O_7)_2$, are relatively high as compared to that in the oxide lattice (Ti_2O_3) and phosphate lattice ($TiPO_4$). It is evident that the matrix effect (anion–anion repulsion) plays an important role in the stabilization of the low valent transition metal cations. Lastly, we believe that the second electropositive cation, Ba^{2+}

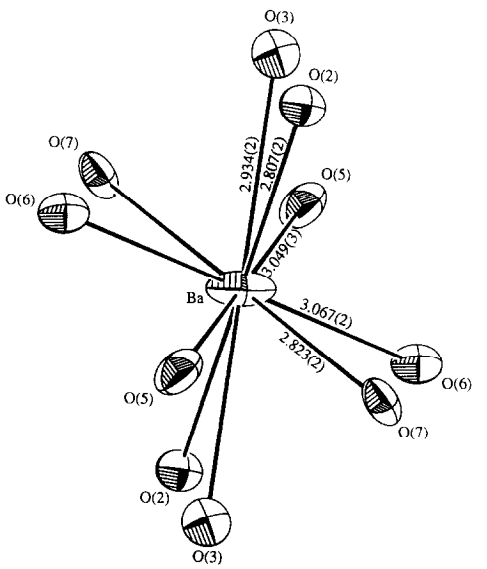

FIG. 8. The coordination of oxygen atoms around Ba^{2+} in $BaTi_2(P_2O_7)_2$.

in this case, not only influences the framework formation but also induces the low oxidation state of titanium cations.

Acknowledgments

This research was supported by the Petroleum Research Fund, administered by the ACS (Grant ACS-PRF No. 21154-G3) and in part by a Rice University startup grant. Financial support for the single crystal X-ray diffractometer by the National Science Foundation is gratefully acknowledged. The authors are indebted to Professor K. R. Poeppelmeier, Mr. M. Anderson, and Mr. J. Vaughey for the magnetic susceptibility measurements.

References

1. H. Y.-P. Hong, *Mater. Res. Bull.* **11,** 173 (1976).
2. J. B. Goodenough, H. Y.-P. Hong, and J. A. Kafalas, *Mater. Res. Bull.* **11,** 204 (1976).
3. Y.-F. Y. Yao and J. T. Kummer, *J. Inorg. Nuclear Chem.* **29,** 2453 (1967).
4. M. S. Whittingham, *J. Chem. Phys.* **54,** 414 (1971).
5. J. L. Briant and G. C. Farrington, *J. Solid State Chem.* **33,** 385 (1980).
6. E. Wang, F. Rinaldi, and M. Greenblatt, *Mat. Res. Bull.* **23,** 113 (1988).
7. A. Leclaire, A. Benmoussa, M. M. Borel, A. Grandin, and B. Raveau, *J. Solid State Chem.* **77,** 299 (1988).
8. A. Nadiri, Ph.D. Dissertation, University of Bordeaux, France, 1986.
9. A. Leclaire, A. Benmoussa, M. M. Borel, A. Grandin, and B. Raveau, *J. Solid State Chem.* **78,** 227 (1989).
10. A. Benmoussa, M. M. Borel, A. Grandin, A. Leclaire, and B. Raveau, *Ann. Chim. Fr.* **14,** 181 (1989).
11. A. Benmoussa, M. M. Borel, A. Grandin, and B. Raveau, *J. Solid State Chem.* **84,** 299 (1990).
12. Ba_2TiO_4, No. 38-1481, Joint Committee on Powder Diffraction Standards, Swarthmore, PA.
13. "TEXSAN: Single Crystal Structure Analysis software, Version 5.0," Molecular Structure Corp., The Woodlands, TX (1989).
14. G. M. Sheldrick, *in* "Crystallographic Computing 3" (G. M. Sheldrick, C. Krüger, and R. Goddard, Eds.), PP. 175–189, Oxford University Press, London/New York (1985).
15. F. Takusagawa, Ames laboratory, Iowa State University, Ames, Iowa, unpublished research, 1981.
16. (a) $BaTiP_2O_8$, No. 25-81, Joint Committee on Powder Diffraction Standards, Swarthmore, PA. (b) TiP_2O_7, No. 38-1468, Joint Committee on Powder Diffraction Standards, Swarthmore, PA.
17. U. Costantino and A. La Ginestra, *Thermochim. Acta* **58,** 179 (1982).
18. R. D. Shannon, *Acta Crystallogr.* **A32,** 751 (1976).
19. W. H. Baur, *Trans. Amer. Crystallogr. Assoc.* **6,** 129 (1970).